^{18}F-Fluoroestradiol PET Imaging of Activating Estrogen Receptor-α Mutations in Breast Cancer

Manoj Kumar[1], Kelley Salem[1], Ciara Michel[1], Justin J. Jeffery[2], Yongjun Yan[1,3], and Amy M. Fowler[1–3]

[1]*Department of Radiology, University of Wisconsin School of Medicine and Public Health, Madison, Wisconsin;* [2]*University of Wisconsin Carbone Cancer Center, Madison, Wisconsin; and* [3]*Department of Medical Physics, University of Wisconsin School of Medicine and Public Health, Madison, Wisconsin*

The purpose of this study was to determine the effect of estrogen receptor-α gene (*ESR1*) mutations at the tyrosine (Y) 537 amino acid residue within the ligand binding domain on ^{18}F-fluoroestradiol (^{18}F-FES) binding and *in vivo* tumor uptake compared with wild-type (WT)-estrogen receptor α (ER). **Methods:** ER-negative MDA-MB-231 breast cancer cells were used to generate stable cell lines that express WT-ER, Y537S, or Y537C mutant ER. Receptor expression and localization were confirmed by Western blot and immunofluorescence, respectively. ER transcriptional function was measured using an estrogen response element-luciferase reporter gene assay and quantitative polymerase chain reaction analysis of ER-regulated endogenous target genes. Saturation binding and competition assays were performed to determine equilibrium dissociation constant (K_d) and half maximal inhibitory concentration (IC50) values. ^{18}F-FES uptake was measured in tumor xenografts grown in female athymic nude mice by small-animal PET/CT imaging and tissue biodistribution using 5.55 MBq (150 μCi) of ^{18}F-FES. A 10-fold-lower injected dose of 0.555 MBq (15 μCi) of ^{18}F-FES was also used for tissue biodistribution. Statistical significance was determined using ANOVA. **Results:** Y537S and Y537C mutations resulted in increased ER transcriptional activity in the absence of estrogen compared with WT-ER (11.48 ± 2.42 fold; $P = 0.0002$, and 5.89 ± 0.94 fold; $P = 0.04$, respectively). Constitutive ER activation of two target genes (*PGR* and *TFF1*) in the absence of estrogen was also observed in Y537S- and Y537C-ER cells compared with WT-ER. K_d values for ^{18}F-FES were 0.98 ± 0.54 nM for Y537S-ER ($P = 0.27$) and 0.24 ± 0.03 nM for Y537C-ER ($P = 0.95$) compared with 0.07 ± 0.03 nM for WT-ER. IC50 values were 0.22 ± 0.09 nM for Y537S-ER ($P = 0.97$), 0.18 ± 0.09 nM for Y537C-ER ($P = 0.99$), and 0.19 ± 0.11 nM for WT-ER. Tumor xenografts expressing Y537S-ER (mean percentage injected dose per gram, 1.45 ± 0.06; $P = 0.77$) and Y537C-ER (2.09 ± 0.20; $P = 0.21$) had similar ^{18}F-FES uptake compared with WT-ER (1.68 ± 0.12). Comparable ^{18}F-FES uptake between Y537S-, Y537C-, and WT-ER xenografts was also observed using a 10-fold-lower injected dose with the tissue biodistribution assay. **Conclusion:** Since tumoral uptake of ^{18}F-FES is not significantly impacted by Y537S-ER or Y537C-ER mutations, the potential diagnostic utility of ^{18}F-FES PET imaging is expected to be equally valid for patients with or without these activating *ESR1* mutations.

Key Words: breast cancer; estrogen receptor mutation; positron emission tomography; ^{18}F-fluoroestradiol; tumor xenografts

J Nucl Med 2019; 60:1247–1252
DOI: 10.2967/jnumed.118.224667

Mutations in the estrogen receptor-α gene (*ESR1*) identified in up to 40% of patients with metastatic estrogen receptor α (ER)–positive breast cancer have been shown to be partially resistant to endocrine therapy and correlate with reduced survival (*1,2*). The majority are missense mutations in the ligand binding domain, frequently involving amino acid residues 536 to 538 in the loop between α-helices 11 and 12, reviewed by Katzenellenbogen et al. (*3*). These gain-of-function mutations allow ER to adopt a conformational change that mimics the agonist-bound receptor and bypass the requirement for estrogen binding to activate ER in a constitutive, ligand-independent manner (*4–6*).

ER imaging using PET with 16α-^{18}F-fluoro-17β-estradiol (^{18}F-FES) is a method to quantify ER across metastatic sites, optimize doses of ER blocking agents, and may predict antiestrogen therapy response (*7*). Tumoral uptake of ^{18}F-FES correlates well with ER protein measured by immunohistochemistry (*8,9*). When the maximum standardized tumoral uptake value of ^{18}F-FES is less than 1.5 to 2.0, patients are unlikely to achieve clinical benefit from endocrine therapy (*10–14*). Residual ER availability detected with ^{18}F-FES PET imaging during ER antagonist therapy may be associated with early disease progression (*15*).

Conformational changes in the ER ligand binding domain of constitutively active mutants cause reduced binding affinities to 17β-estradiol (E2) using tritiated-estradiol in radioligand binding assays (*4,16*). Given the structural similarities between E2 and ^{18}F-FES (*17*), we hypothesized that *ESR1* activating mutations at the Y537 amino acid residue will have reduced ^{18}F-FES binding compared with wild-type (WT)-ER. This question has important clinical relevance because *ESR1* mutations could possibly lead to a false-negative PET imaging result if they cause reduced ^{18}F-FES binding affinity. The purpose of this study was to determine the effect of *ESR1* mutations at Y537 within the ligand binding domain on ^{18}F-FES binding and *in vivo* tumor uptake compared with WT-ER.

MATERIALS AND METHODS

Cell Culture

Experiments were performed according to a protocol approved by the Office of Biologic Safety. Human ER-negative breast cancer

Received Dec. 18, 2018; revision accepted Feb. 6, 2019.
For correspondence or reprints contact: Amy M. Fowler, University of Wisconsin School of Medicine and Public Health, 600 Highland Ave., Madison, WI 53792-3252.
E-mail: afowler@uwhealth.org
Published online Mar. 8, 2019.

cells (MDA-MB-231) were authenticated using short tandem repeat analysis and tested negative for murine pathogens and *Mycoplasma* contamination (IDEXX BioResearch). Cells were cultured in Dulbecco's modified Eagle medium (Corning) with 10% fetal bovine serum (VWR) and 1% penicillin and streptomycin (Gibco) at 37°C and 10% CO_2.

Constructs and Transfection

Y537C and Y537S mutations were introduced into WT human *ESR1* in pBluescript cloning vector (Stratagene) using a site-directed polymerase chain reaction mutagenesis kit (Agilent Technologies) and primers listed in Supplemental Table 1 (supplemental materials are available at http://jnm.snmjournals.org). Generated mutations were verified by Sanger sequencing using primers listed in Supplemental Table 2. The complementary DNA for these receptors were inserted into a tetracycline-inducible expression vector (pUHD10-3) (*18*). Mutant and WT *ESR1* sequences were reverified using the primers indicated in Supplemental Table 2. Doxycycline-inducible MDA-MB-231 cell lines were generated by first stably transfecting cells with a plasmid containing the reverse tet-transactivator construct (pUHD172-1 neo) (*19*). Positive colonies were identified using a tetracycline responsive element-luciferase reporter assay. Clones with strong reporter gene induction with doxycycline were stably cotransfected with the pUHD10-3 expression vectors containing mutant or WT-ER and a puromycin resistance plasmid (pBABE-puro). Transfected cells were maintained with G418 (40 μg/mL; Gemini Bio-Products) and puromycin (1 μg/mL; Sigma-Aldrich).

Western Blot Analysis

Whole-cell lysates were prepared from cell pellets or crushed flash-frozen tumors using radioimmunoprecipitation assay buffer (Sigma) with 2 mM sodium orthovanadate, protease (1:500) and phosphatase (1:100) inhibitor cocktails (Sigma). Protein concentration was determined with Bradford assay (Bio-Rad). Equal amounts of protein were run on 7.5% sodium-dodecyl sulfate-polyacrylamide gel electrophoresis (Bio-Rad) and transferred to a polyvinylidene difluoride membrane (Millipore). Saturating amounts of antibodies were used for ER (1:1,000 clone SP1; ThermoFisher), β-actin (1:10,000; Sigma), and horseradish peroxidase–conjugated IgG (1:3,000; GE Healthcare). Bands for ER protein were quantified using GeneTools software (Syngene) and were normalized to β-actin loading control. Full-length recombinant human ERα protein (Invitrogen) was used to generate standard curves for semiquantitative analysis, as described previously (*20*). Molar concentrations of ER in the cell lines and tumors were calculated using linear regression (r^2 values ranged from 0.95 to 0.99) and are expressed as fmol/mg total protein.

Immunofluorescence

Doxycycline-treated cells were seeded in chamber slides (Sarstedt) and then fixed with 2% formaldehyde, permeabilized with 0.5% Triton X-100 (Sigma), blocked with 10% goat serum for 1 h at 37°C, and incubated with anti-ER antibody (1:100, Clone 6F11; Leica), overnight at 4°C. Slides were then probed with AlexaFluor 488 antimouse antibody (1:100, Life Technologies) for 1 h at room temperature. Slides were mounted with ProLong Gold Antifade with 4′6-diamidino-2-phenylindole (DAPI) (Life Technologies) and imaged with confocal microscopy (Nikon A1RS).

Transcriptional Reporter Gene Assay

Cells were grown in steroid hormone-depleted medium (10% charcoal/dextran stripped fetal bovine serum in phenol red-free medium with 1% penicillin/streptomycin and 2% L-glutamine) for 3 d then were seeded in a 6-well plate (5×10^5 cells/well). The following day, cells were cotransfected with estrogen receptor response element (ERE)-luciferase (0.75 μg) and cytomegalovirus-β-galactosidase (0.25 μg) reporter plasmids using Lipofectamine 3000 (Life Technologies) and treated with doxycycline (5 μg/mL; Sigma) to induce ER expression. The next day, cells were treated with ethanol (vehicle) or 10 nM 17β-estradiol (E2, Sigma) for 24 h. Luciferase activity (Promega) and β-galactosidase activity (Tropix) were measured according to the manufacturers' protocols.

Quantitative Polymerase Chain Reaction

Estrogen-deprived cells were seeded in a 6-well plate and were supplemented with doxycycline (5 μg/mL) overnight. The next day, cells were treated with ethanol or 10 nM E2 for 24 h. RNA was isolated (RNeasy kit; Qiagen) and complementary DNA was generated (iScript cDNA kit; BioRad). Primers for messenger RNA of progesterone receptor (PGR), trefoil factor-1 (TFF1), and ribosomal protein 36B4, which is a reference/house-keeping gene, are stated in Supplemental Table 3.

^{18}F-FES Cell Uptake Assays

Saturation binding assays were performed by first seeding 1×10^5 cells in duplicate 24-well plates. The following day, cells were washed with phosphate-buffered saline and placed in stripped serum medium with doxycycline (5 μg/mL). On day 3 immediately before adding ^{18}F-FES, one plate was treated with ethanol control and the other was treated with 1×10^{-8} M 17β-estradiol (E2; Sigma). Increasing concentrations of ^{18}F-FES, 0.002–0.22 MBq (0.06–6 μCi), were then added to the respective wells. For the competition binding assay, increasing amounts of cold E2 (1×10^{-13} to 1×10^{-7} M) were added before the addition of 0.037 MBq (1 μCi) of ^{18}F-FES and incubated for 1 h at 37°C. Cells were harvested, and radioactivity was measured and analysis performed as described previously (*17*). The equilibrium dissociation constant (K_d) and half-maximal inhibitory concentration (IC50) were determined using nonlinear regression (binding saturation one-site-total and nonspecific binding for K_d and binding-competitive one-site-fit for IC50) with GraphPad Prism 6.05 software.

Tumor Xenografts

Experiments were performed according to the American Association for Laboratory Animal Science guidelines following an approved protocol by the Institutional Animal Care and Use Committee. Adult female NCr-*nu/nu* mice aged 6 wk (Charles River) were orthotopically injected with 1.5×10^6 cells at a 1:1 ratio with Matrigel (BD Biosciences) into the bilateral thoracic mammary fat pads (20 mice for ^{18}F-FES biodistribution and 14 mice for PET/CT imaging). Palpable tumors were observed after 4 d, and tumor growth was monitored twice a week. Mice were supplemented with doxycycline (1 mg/mL) in the drinking water 2 d before experiments to induce ER expression. Tumor size was measured by calipers and volume calculated by (length × width^2)/2.

Histology

Excised tumors were fixed in 10% formalin, embedded in paraffin, and sectioned. Slides were deparaffinized followed by heat epitope retrieval in citrate buffer (pH 6.0) for 60 min at 95°C. Immunostaining was performed for ER (1:100 clone SP1; ThermoFisher) using VECTASTAIN ABC HRP Kit (Vector Laboratories). Hematoxylin and eosin staining was also performed. Slides were scanned at 20× magnification using a whole-slide bright field imaging system (Aperio Image Scope software).

PET/CT Imaging and Tissue Biodistribution

^{18}F-FES was synthesized using previously described methods (*17*). Average molar activity at the end of synthesis was 271 GBq/μmol (115–393 GBq/μmol; 7,337 mCi/μmol [3,111–10,634 mCi/μmol]).

For imaging, nonfasted mice were injected in the tail vein with 5.55 MBq (150 μCi) of ^{18}F-FES. All mice were anesthetized with 1.5%–2.0% isoflurane and scanned supine in a microPET/CT scanner (Inveon; Siemens Preclinical Solutions) 1 h after tail vein injection. CT imaging lasted 12 min (2 bed positions × 6 min) followed by PET image acquisition (40 million counts/mouse; typically, <10 min) using 1 PET bed position. PET data were histogrammed into 1 static frame and reconstructed using ordered-subset expectation maximization of 3 dimensions followed by the maximum a posteriori algorithm (18 iterations, 16 subsets). CT attenuation and scatter correction were applied. PET/CT images were automatically coregistered and analyzed using Inveon Research Workplace 3.0 (Siemens Medical Solutions). Regions of interest were drawn around the tumor and within quadricep muscles. Data are expressed as the mean percentage injected dose per gram (%ID/g). The tumor-to-muscle ratio was calculated as the ratio of the mean %ID/g of tumor to that of averaged left and right quadricep muscles.

For the tissue biodistribution assay, tumor-bearing mice were injected with either 0.555 MBq (15 μCi) or 5.55 MBq (150 μCi) of ^{18}F-FES via the tail vein. Blood and tissues (tumors, left and right quadricep muscles, heart, slice of liver, and uterus) were harvested and weighed 1 h after tail vein injection. Radioactivity was measured using a γ-counter, and data were background-corrected to calculate the %ID/g. Tumor-to-muscle ratio was calculated as the ratio of the mean %ID/g of tumor to that of averaged left and right quadricep muscles.

Statistics

Statistical significance was determined using unpaired *t* tests when comparing the means of 2 unmatched groups and one-way ANOVA with Tukey post-test when comparing the means of more than 2 unmatched groups (GraphPad Prism 6.05). Results are presented as mean ± SEM. $P < 0.05$ was considered significant.

RESULTS

ER Expression and Localization in the Generated Breast Cancer Cell Lines

ER protein levels increased in a dose-dependent manner with doxycycline (Figs. 1A and 1B). Quantified ER protein levels in the mutant cell lines were not statistically different compared with WT-ER at any of the tested doses ($P \geq 0.05$). Appropriate nuclear localization of ER protein was observed in WT-ER, Y537C-ER, and Y537S-ER cells (Fig. 1C). No detectable ER expression was observed in the parental ER-negative cells.

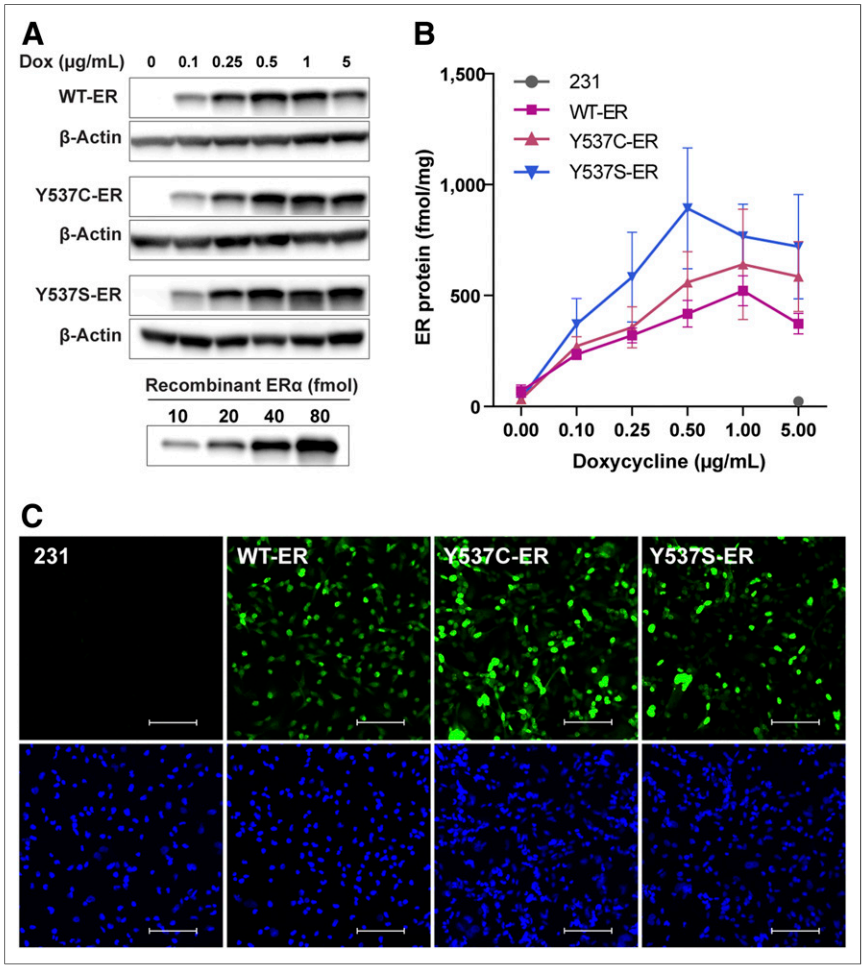

FIGURE 1. ER protein expression and localization in generated breast cancer cell lines. (A) Representative Western blot of ER protein in WT-ER, Y537C-ER, and Y537S-ER cells treated with increasing doses of doxycycline for 24 h. (B) ER protein quantification (mean ± SEM) from 3 independent experiments. (C) Immunofluorescence for ER localization: Alexa fluor 488 staining for ER (top) and DAPI nuclear staining (bottom). Scale bar = 100 μm. Images are representatives of 3 individual experiments.

Constitutive Transcriptional Activity of Y537C-ER and Y537S-ER

Compared with WT-ER, the Y537C-ER and Y537S-ER mutants demonstrated significantly higher transcriptional activity in the presence and absence of estrogen (Fig. 2A). The transcriptional activities of Y537C-ER and Y537S-ER were 5.89 ± 0.94 fold ($P = 0.04$) and 11.48 ± 2.42 fold ($P = 0.0002$) higher than WT-ER, respectively, in the absence of estrogen (Fig. 2B). Transcription of endogenous target ER genes was also higher in cells expressing mutant receptors compared with WT-ER in the absence of estrogen (Figs. 2C and 2D). PGR messenger RNA expression was increased 3.11 ± 0.43 fold ($P = 0.0005$) for Y537C-ER and 8.49 ± 1.88 fold ($P = 0.0019$) for Y537S-ER compared with WT-ER. TFF1 messenger RNA expression was increased 3.40 ± 0.71 fold ($P = 0.0055$) for Y537C-ER and 9.60 ± 2.22 fold ($P = 0.0022$) for Y537S-ER compared with WT-ER.

Binding Affinities of Y537C-ER and Y537S-ER for ^{18}F-FES

^{18}F-FES binding affinity was reduced in cells expressing Y537C-ER and Y537S-ER compared with WT-ER (Supplemental Fig. 1); however, this was not statistically significant (K_d: 0.24 ± 0.03 nM for Y537C-ER, $P = 0.95$; 0.98 ± 0.54 nM for Y537S-ER, $P = 0.27$ vs. 0.07 ± 0.03 nM for WT-ER).

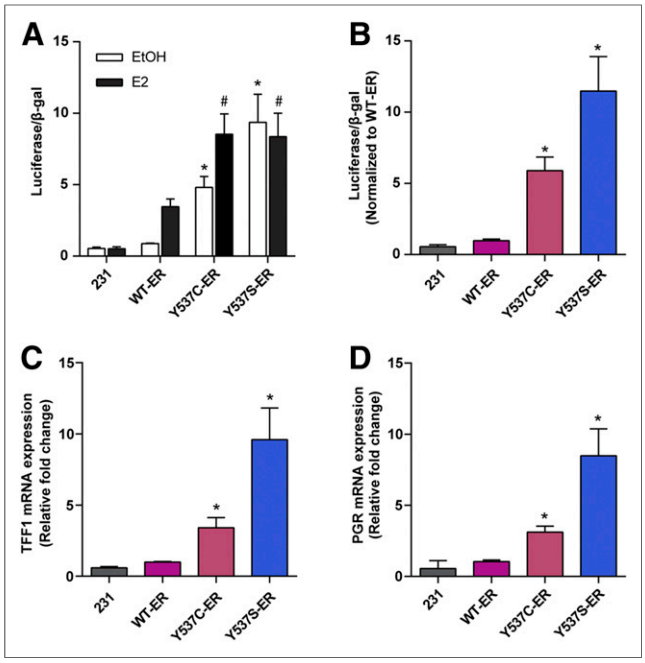

FIGURE 2. Transcriptional activity of Y537C-ER and Y537S-ER compared with WT-ER. (A) Parental ER-negative MDA-MB-231, WT-ER, Y537C-ER, and Y537S-ER cells were estrogen-deprived and transfected with ERE-luciferase and β-galactosidase plasmids and then treated with ethanol (EtOH) vehicle or 10 nM 17β-estradiol (E2) for 24 h. ERE-luciferase reporter gene activity was measured and normalized to β-galactosidase activity. $^*P < 0.05$ compared with ethanol-treated WT-ER; #$P < 0.05$ compared with E2-treated WT-ER. (B) Transcriptional activity normalized to WT-ER in the absence of E2. Expression of ER-regulated target genes, *TFF1* (C) and *PGR* (D), was measured in estrogen-deprived cells after 24 h treatment with ethanol vehicle control. Values represent the mean ± SEM of 3 independent experiments. $^*P < 0.05$ compared with WT-ER.

IC50 values (Supplemental Fig. 2) were comparable between the cell lines: 0.18 ± 0.09 nM for Y537C-ER ($P = 0.99$), 0.22 ± 0.09 nM for Y537S-ER ($P = 0.97$), and 0.19 ± 0.11 nM for WT-ER.

^{18}F-FES PET/CT Imaging and Tissue Biodistribution of Tumor Xenograft–Bearing Mice

Mean tumor volumes of the ER-negative parental MDA-MB-231, WT-ER, Y537C-ER, and Y537S-ER xenografts at the time of imaging were 105 ± 5 mm^3, 112 ± 30 mm^3, 99 ± 12 mm^3, and 145 ± 30 mm^3, respectively. ^{18}F-FES uptake in the ER mutant tumors was similar to WT-ER xenografts (Fig. 3A). The mean %ID/g tumor uptake values were 1.68 ± 0.12 for WT-ER, 2.09 ± 0.20 ($P = 0.21$) for Y537C-ER, and 1.45 ± 0.06 for Y537S-ER tumors ($P = 0.77$) (Fig. 3B). Tumor-to-muscle ratios were 3.12 ± 0.45 for WT-ER, 3.44 ± 0.25 ($P = 0.86$) for Y537C-ER, and 2.56 ± 0.17 ($P = 0.60$) for Y537S-ER (Fig. 3C). Excised tumors had comparable ER protein levels: 706 ± 136 fmol/mg protein for WT-ER, 771 ± 110 for Y537C-ER ($P = 0.97$), and 585 ± 68 for Y537S-ER ($P = 0.86$).

To confirm that tumor specific uptake of ^{18}F-FES is not confounded due to possible saturation of the receptor by the amount of injected mass dose, a tissue biodistribution assay was performed using 2 different ^{18}F-FES doses. At 5.55 MBq (150 μCi; the injected dose that was used for PET/CT imaging), we estimated approximately 5% receptor occupancy with ^{18}F-FES based on an average specific activity of 271 GBq/μmol (7,337 mCi/μmol), approximately 1.5 %ID/g of tumor tissue, and approximately 600 fmol ER per mg total protein. At 0.555 MBq (15 μCi), we simulated 10-fold-lower receptor occupancy (~0.5%). Tumoral ^{18}F-FES uptake was not significantly affected by the Y537 mutations with either of the injected doses tested (Figs. 4A and 4B), which is consistent with the PET/CT results. ER protein expression in the excised tumors was comparable (Figs. 4C and 4D; Supplemental Fig. 3). Complete tissue biodistribution data are included in Supplemental Figure 4. Because the %ID/g values were not significantly different between the two injected doses, this provides further evidence that the mass dose of injected ^{18}F-FES is not saturating the receptor.

DISCUSSION

Many studies have evaluated ^{18}F-FES PET imaging as a method for quantifying ER expression, predicting response to therapy, and optimizing doses of ER blocking agents (*8–15*). Their results provide the rationale for an ongoing multi-institutional validation trial in the United States and increasing clinical use in Europe of ^{18}F-FES PET as an additional diagnostic tool when conventional imaging is inconclusive (*21,22*). Given the prevalence of *ESR1* mutations in

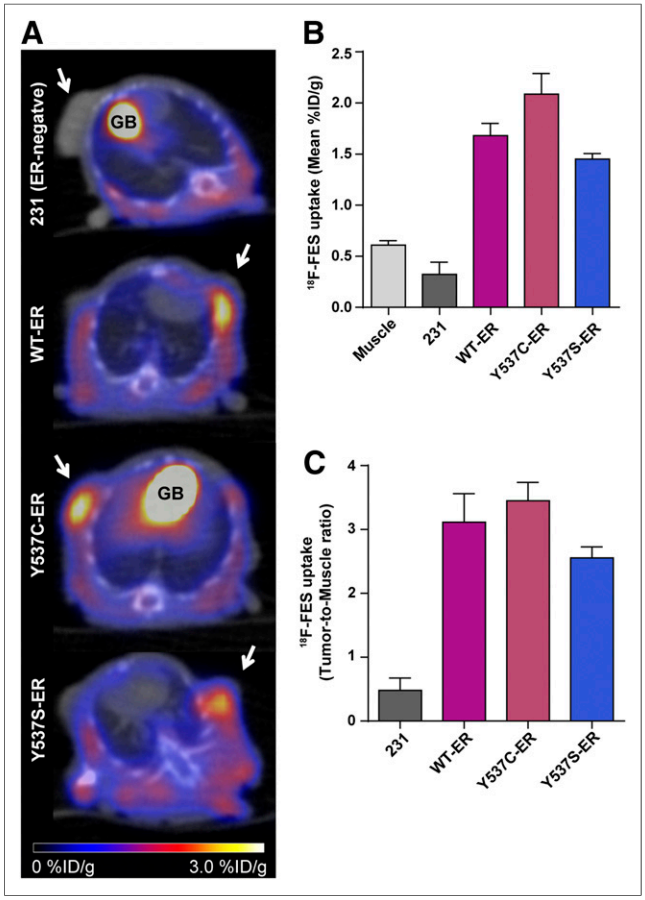

FIGURE 3. ^{18}F-FES PET/CT imaging of Y537C-ER and Y537S-ER tumor xenografts compared with WT-ER. (A) Representative axial PET/CT images of mice bearing tumors of parental ER-negative MDA-MB-231, WT-ER, Y537C-ER, and Y537S-ER cell lines ($n = 3$, 5, 9 and 6, respectively) imaged at 1 h after tail vein injection with 5.55 MBq (150 μCi) of ^{18}F-FES. Mice were imaged 18 d after tumor cell injection. Tumors are indicated by arrows. Physiologic uptake in gallbladder is labeled as GB. ^{18}F-FES uptake in muscle and tumor xenografts quantified as mean %ID/g (B) and tumor-to-muscle ratio (C). Values represent mean ± SEM.

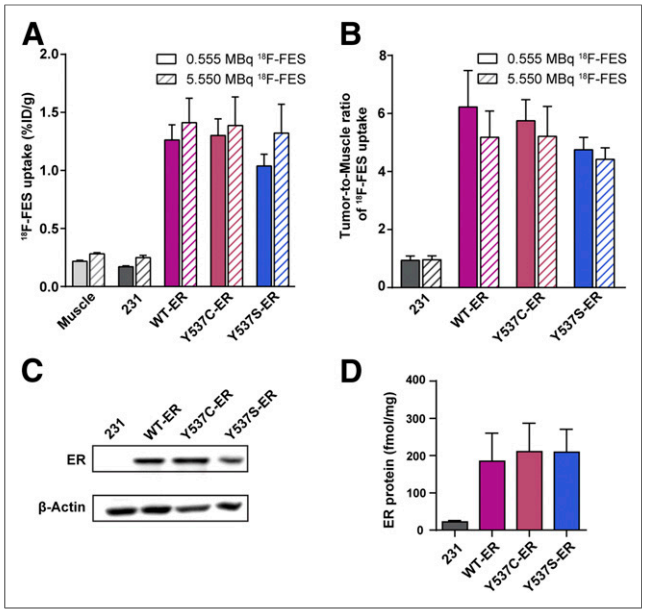

FIGURE 4. ^{18}F-FES uptake in Y537C-ER and Y537S-ER tumor xenografts compared with WT-ER at 10-fold-lower injected dose. Mean %ID/g (A) and tumor-to-muscle uptake ratios (B) of ^{18}F-FES at 0.555 MBq (15 μCi) and 5.55 MBq (150 μCi) injected doses in tumor-bearing mice 1 h after tail vein injection. For 0.555 MBq of ^{18}F-FES, the number of tumors were $n = 4$ for MDA-MB-231, $n = 6$ for WT-ER, $n = 5$ for Y537C-ER, and $n = 5$ for Y537S-ER. For 5.55 MBq of ^{18}F-FES, the number of tumors were $n = 4$ for MDA-MB-231, $n = 5$ for WT-ER, $n = 4$ for Y537C-ER, and $n = 5$ for Y537S-ER. The biodistribution assay was performed 28 d after tumor cell injection. Values represent mean ± SEM. Statistical comparisons in A are as follows for 0.555 MBq of ^{18}F-FES: Y537C-ER vs. WT-ER, $P > 0.99$; Y537S-ER vs. WT-ER, $P = 0.75$, and for 5.55 MBq of ^{18}F-FES: Y537C-ER vs. WT-ER, $P > 0.99$; Y537S-ER vs. WT-ER, $P = 0.99$. Representative Western blot for ER protein (C) and ER protein quantification (D) from excised tumors.

metastatic breast cancer, it is plausible that *ESR1* mutations may contribute to the reported diversity between ^{18}F-FES uptake both within and among patients (*23–25*) and could result in a false-negative PET imaging result if these mutations impair ^{18}F-FES binding. To the best of our knowledge, the potential impact of activating *ESR1* mutations on the accuracy of ^{18}F-FES PET imaging has not been investigated.

Previously, we showed that substitution of a single amino acid residue at glycine 521 to arginine in the ER ligand binding pocket completely abolishes ^{18}F-FES binding (*26*). This was an expected result because the ER ligand binding domain crystal structure indicates that the D-ring of 17β-estradiol makes nonpolar contacts with G521, which are essential for agonist binding (*27,28*). Here, we tested the hypothesis that mutations at Y537 in helix 12 of the ER ligand binding domain would result in decreased ^{18}F-FES binding and tumor uptake. Unlike the G521R mutation, the expected effect of Y537 mutations is less obvious because Y537 is not directly involved in estradiol binding. Structural data indicate that unliganded Y537S-ER mimics the closed ligand binding pocket conformation of agonist-bound WT-ER and has slower ligand association and dissociation rates (*5,29*). Thus, constitutively active *ESR1* mutations affect receptor conformation and may alter ^{18}F-FES access to the ligand binding pocket. Using xenografts from engineered breast cancer cell lines, we found equivalent ^{18}F-FES uptake between WT-ER and Y537C-ER or Y537S-ER mutant tumors by PET/CT and biodistribution experiments.

Although the binding affinities of Y537C-ER and Y537S-ER for ^{18}F-FES tended to be less than WT-ER, there was no statistically significant difference. Also, there was no difference in IC50 values obtained from competitive binding assays. This was unexpected because previous studies showed decreased binding affinity of Y537S-ER for tritiated estradiol compared with WT-ER (*4,16*). A likely reason for the discrepancy is that previous studies used *in vitro* purified ER ligand binding domains. In contrast, ^{18}F-FES binding assays performed in our study used intact cells expressing full-length receptors. Our results are more consistent with Carlson et al., which showed similar K_ds for tritiated estradiol when full-length receptor was used (*5*).

The clinical use of tumor genomic sequencing is growing for patients with advanced breast cancer. However, it is not yet considered standard-of-care given the lack of *ESR1* mutation-specific therapy regimens (*30*). Thus, patients in ^{18}F-FES imaging trials are a heterogeneous mix of those with and without *ESR1* mutations. Our results indicate that *ESR1* mutations at Y537C and Y537S are not detrimental to ^{18}F-FES binding and tumor uptake. These findings support the utility of ^{18}F-FES PET imaging and its validity as a diagnostic tool for ER-positive patients with or without these specific *ESR1* mutations. However, the positive predictive value of ^{18}F-FES PET for endocrine therapy response may be decreased for patients with activating *ESR1* mutations if these lesions are indistinguishable from WT-ER because those tumors are more endocrine-resistant. This hypothesis requires further investigation. Radiopharmaceuticals that probe downstream targets of ER action, such as ^{18}F-fluorofuranylnorprogesterone for PGR (*31*), may be more suitable for early therapy response assessment in patients with *ESR1* mutations.

Because the allele frequency of somatic *ESR1* mutations ranges from 1% to 45%, a heterogeneous population of both WT and mutant receptors exists in a single tumor (*2*). For this study, the effect of Y537S and Y537C mutations was tested in isolation from the WT receptor. Although this design does not exactly recapitulate conditions seen in patients and is a potential limitation, it does allow for a more direct examination of the effect of the mutant receptor without confounding effects from endogenous WT-ER. Also, we have limited our conclusions to the 2 *ESR1* activating mutations tested in this study. It is possible that other hotspot mutations, such as Y537N and D538G, may have different results.

CONCLUSION

Tumoral uptake of ^{18}F-FES is not significantly impacted by Y537C or Y537S activating *ESR1* mutations. The potential diagnostic utility of ^{18}F-FES PET imaging is expected to be equally valid for patients with or without these specific *ESR1* mutations.

DISCLOSURE

This work was supported by the Clinical and Translational Science Award program, through the NIH National Center for Advancing Translational Sciences (grant UL1TR002373) and the UW Institute of Clinical and Translational Research KL2 Scholar Award (1KL2TR002374). The content is solely the responsibility of the authors and does not necessarily represent the official views of the NIH. The research was also supported by the Philips Healthcare/Radiological Society of North America Research Seed Grant (#RSD1420), the UW Paul P. Carbone Cancer Center Young Investigator Award, the American Cancer Society Institutional Research Grant Pilot Award (IRG-15-213-51), and a Mary Kay

Innovative Innovative/Translational Cancer Research Grant. We thank the UW Optical Imaging Core, the Translational Research Initiatives in Pathology laboratory, in part supported by the UW Department of Pathology and Laboratory Medicine and UWCCC grant (P30 CA014520), and the Experimental Pathology Laboratory (P30 CA014520) for their services. Amy M. Fowler receives research support from GE Healthcare for PET/MRI research. No other potential conflict of interest relevant to this article was reported.

ACKNOWLEDGMENTS

We thank the UW-Madison Cyclotron Laboratory for ^{18}F production, the Radiopharmaceutical Production Facility for ^{18}F-FES synthesis, and the Small Animal Imaging Facility for technical support.

KEY POINTS

QUESTION: What is the effect of clinically relevant mutations in estrogen receptor-α on ^{18}F-FES binding and *in vivo* tumor uptake?

PERTINENT FINDINGS: ^{18}F-FES uptake was not significantly different between Y537S-, Y537C-, and wild-type ER–expressing breast cancer cell lines and tumor xenografts.

IMPLICATIONS FOR PATIENT CARE: The potential diagnostic utility of ^{18}F-FES PET imaging is expected to be equally valid for patients with or without these types of activating *ESR1* mutations.

REFERENCES

1. Chandarlapaty S, Chen D, He W, et al. Prevalence of ESR1 mutations in cell-free DNA and outcomes in metastatic breast cancer: a secondary analysis of the BOLERO-2 clinical trial. *JAMA Oncol.* 2016;2:1310–1315.
2. Fribbens C, O'Leary B, Kilburn L, et al. Plasma ESR1 mutations and the treatment of estrogen receptor-positive advanced breast cancer. *J Clin Oncol.* 2016; 34:2961–2968.
3. Katzenellenbogen JA, Mayne CG, Katzenellenbogen BS, Greene GL, Chandarlapaty S. Structural underpinnings of oestrogen receptor mutations in endocrine therapy resistance. *Nat Rev Cancer.* 2018;18:377–388.
4. Fanning SW, Mayne CG, Dharmarajan V, et al. Estrogen receptor alpha somatic mutations Y537S and D538G confer breast cancer endocrine resistance by stabilizing the activating function-2 binding conformation. *Elife.* 2016;5: e12792.
5. Carlson KE, Choi I, Gee A, Katzenellenbogen BS, Katzenellenbogen JA. Altered ligand binding properties and enhanced stability of a constitutively active estrogen receptor: evidence that an open pocket conformation is required for ligand interaction. *Biochemistry.* 1997;36:14897–14905.
6. Weis KE, Ekena K, Thomas JA, Lazennec G, Katzenellenbogen BS. Constitutively active human estrogen receptors containing amino acid substitutions for tyrosine 537 in the receptor protein. *Mol Endocrinol.* 1996;10:1388–1398.
7. Linden HM, Peterson LM, Fowler AM. Clinical potential of estrogen and progesterone receptor imaging. *PET Clin.* 2018;13:415–422.
8. Mintun MA, Welch MJ, Siegel BA, et al. Breast cancer: PET imaging of estrogen receptors. *Radiology.* 1988;169:45–48.
9. Peterson LM, Mankoff DA, Lawton T, et al. Quantitative imaging of estrogen receptor expression in breast cancer with PET and ^{18}F-fluoroestradiol. *J Nucl Med.* 2008;49:367–374.
10. van Kruchten M, de Vries EGE, Brown M, et al. PET imaging of oestrogen receptors in patients with breast cancer. *Lancet Oncol.* 2013;14:e465–e475.
11. Mortimer JE, Dehdashti F, Siegel BA, Katzenellenbogen JA, Fracasso P, Welch MJ. Positron emission tomography with 2-[^{18}F]fluoro-2-deoxy-D-glucose and 16alpha-[^{18}F]fluoro-17beta-estradiol in breast cancer: correlation with estrogen receptor status and response to systemic therapy. *Clin Cancer Res.* 1996;2:933–939.
12. Peterson LM, Kurland BF, Schubert EK, et al. A phase 2 study of 16alpha-[^{18}F]-fluoro-17beta-estradiol positron emission tomography (FES-PET) as a marker of hormone sensitivity in metastatic breast cancer (MBC). *Mol Imaging Biol.* 2014;16:431–440.
13. Linden HM, Stekhova SA, Link JM, et al. Quantitative fluoroestradiol positron emission tomography imaging predicts response to endocrine treatment in breast cancer. *J Clin Oncol.* 2006;24:2793–2799.
14. van Kruchten M, Glaudemans A, de Vries EFJ, Schroder CP, de Vries EGE, Hospers GAP. Positron emission tomography of tumour [^{18}F]fluoroestradiol uptake in patients with acquired hormone-resistant metastatic breast cancer prior to oestradiol therapy. *Eur J Nucl Med Mol Imaging.* 2015;42:1674–1681.
15. van Kruchten M, de Vries EG, Glaudemans AW, et al. Measuring residual estrogen receptor availability during fulvestrant therapy in patients with metastatic breast cancer. *Cancer Discov.* 2015;5:72–81.
16. Zhao Y, Laws MJ, Guillen VS, et al. Structurally novel antiestrogens elicit differential responses from constitutively active mutant estrogen receptors in breast cancer cells and tumors. *Cancer Res.* 2017;77:5602–5613.
17. Salem K, Kumar M, Kloepping KC, Michel CJ, Yan Y, Fowler AM. Determination of binding affinity of molecular imaging agents for steroid hormone receptors in breast cancer. *Am J Nucl Med Mol Imaging.* 2018;8:119–126.
18. Gossen M, Bujard H. Tight control of gene expression in mammalian cells by tetracycline-responsive promoters. *Proc Natl Acad Sci USA.* 1992;89:5547–5551.
19. Gossen M, Freundlieb S, Bender G, Muller G, Hillen W, Bujard H. Transcriptional activation by tetracyclines in mammalian cells. *Science.* 1995;268:1766–1769.
20. Fowler AM, Chan SR, Sharp TL, et al. Small-animal PET of steroid hormone receptors predicts tumor response to endocrine therapy using a preclinical model of breast cancer. *J Nucl Med.* 2012;53:1119–1126.
21. Venema CM, Apollonio G, Hospers GA, et al. Recommendations and technical aspects of 16alpha-[^{18}F]fluoro-17beta-estradiol PET to image the estrogen receptor in vivo: the Groningen experience. *Clin Nucl Med.* 2016;41:844–851.
22. van Kruchten M, Glaudemans AW, de Vries EF, et al. PET imaging of estrogen receptors as a diagnostic tool for breast cancer patients presenting with a clinical dilemma. *J Nucl Med.* 2012;53:182–190.
23. Currin E, Peterson LM, Schubert EK, et al. Temporal heterogeneity of estrogen receptor expression in bone-dominant breast cancer: ^{18}F-fluoroestradiol PET imaging shows return of ER expression. *J Natl Compr Canc Netw.* 2016;14: 144–147.
24. Nienhuis HH, van Kruchten M, Elias SG, et al. ^{18}F-Fluoroestradiol tumor uptake is heterogeneous and influenced by site of metastasis in breast cancer patients. *J Nucl Med.* 2018;59:1212–1218.
25. Kurland BF, Peterson LM, Lee JH, et al. Between-patient and within-patient (site-to-site) variability in estrogen receptor binding, measured in vivo by ^{18}F-fluoroestradiol PET. *J Nucl Med.* 2011;52:1541–1549.
26. Salem K, Kumar M, Powers GL, et al. ^{18}F-16alpha-17beta-fluoroestradiol binding specificity in estrogen receptor-positive breast cancer. *Radiology.* 2018;286: 856–864.
27. Brzozowski AM, Pike AC, Dauter Z, et al. Molecular basis of agonism and antagonism in the oestrogen receptor. *Nature.* 1997;389:753–758.
28. Danielian PS, White R, Hoare SA, Fawell SE, Parker MG. Identification of residues in the estrogen receptor that confer differential sensitivity to estrogen and hydroxytamoxifen. *Mol Endocrinol.* 1993;7:232–240.
29. Nettles KW, Bruning JB, Gil G, et al. NFkappaB selectivity of estrogen receptor ligands revealed by comparative crystallographic analyses. *Nat Chem Biol.* 2008; 4:241–247.
30. Van Poznak C, Somerfield MR, Bast RC, et al. Use of biomarkers to guide decisions on systemic therapy for women with metastatic breast cancer: American Society of Clinical Oncology Clinical Practice Guideline. *J Clin Oncol.* 2015;33:2695–2704.
31. Salem K, Kumar M, Yan Y, et al. Sensitivity and isoform specificity of ^{18}F-fluorofuranylnorprogesterone for measuring progesterone receptor protein response to estradiol challenge in breast cancer. *J Nucl Med.* 2019;60:220–226.